LIMNOLOGY AND OCEANOGRAPHY
Letters

ASLO
Open Access

Limnology and Oceanography Letters 2021

doi: 10.1002/lol2.10224

LETTER

Low temperature sensitivity of picophytoplankton P : B ratios and growth rates across a natural 10°C temperature gradient in the oligotrophic Indian Ocean

Michael R. Landry [1]*, *Karen E. Selph* [2], *Raleigh R. Hood* [3], *Claire H. Davies* [4], *Lynnath E. Beckley* [5]

[1]Scripps Institution of Oceanography, University of California at San Diego, La Jolla, California; [2]Department of Oceanography, University of Hawai'i at Manoa, Honolulu, Hawaii; [3]Horn Point Laboratory, University of Maryland Center for Environmental Science, Cambridge, Maryland; [4]CSIRO Oceans and Atmosphere Flagship, Castray Esplanade, Hobart, Tasmania, Australia; [5]Environmental and Conservation Sciences, Murdoch University, Murdoch, Western Australia, Australia

Scientific Significance Statement

Most models and predictions of the oceans under climate warming assume relatively high temperature sensitivities of phytoplankton growth, derived mainly from laboratory studies. Such assumptions are questionable under nutrient limitation, and mortality (loss) factors must also be considered for nutrient-poor waters, where production, nutrient cycling, and biomass turnover need to balance. Our investigation of picophytoplankton biomass (B), production (P), and growth along a natural 10°C temperature gradient in the oligotrophic eastern Indian Ocean reveals low temperature sensitivities of P : B and growth rates, especially for *Prochlorococcus*, the biomass dominant. From documented variability in cell surface properties of *Prochlorococcus* and their effectiveness in reducing grazing vulnerability, we hypothesize that the selection for mortality defenses could be important for understanding microbial adaptations to a warming ocean. We also highlight natural environmental gradients that bridge future conditions in the contemporary ocean as major resources for investigating microbial physiological, genetic, and ecological adaptations and testing hypotheses.

Abstract

We investigated temperature sensitivities of picophytoplankton growth along a natural 10°C (18–28°C) temperature gradient in the eastern Indian Ocean characterized by deep mixing and consistently low dissolved nitrogen. Population biomass (B), cell carbon, and chlorophyll were measured by flow cytometry. Instantaneous growth (μ) and production (P) were calculated from dilution incubations at four light levels. Contrary to most empirical and theoretical predictions, *Prochlorococcus*, the biomass dominant, showed insignificant temperature sensitivity, with nominal Q_{10} values of 1.06 and 1.18 for P : B and μ, respectively, and activation energies (E_a) of 0.05 and 0.12 eV. Q_{10} and E_a values for *Synechococcus* (1.36–1.42 and 0.23–0.27 eV) were also below prediction, and picoeukaryotes showed high variability, including negative rates suggesting lytic cycles, at high

*Correspondence: mlandry@ucsd.edu

Associate editor: Angelicque White

Author Contribution Statement: MRL and LEB conceived the study. MRL, RRH, and CHD conducted the field sampling and experiments. KES did the flow cytometric analyses. MRL analyzed results and drafted the manuscript. All authors contributed to comments and edits of the manuscript.

Data Availability Statement: Data are archived at Dryad site https://datadryad.org/stash/dataset/doi:10.6076/D17C7J and at BCO-DMO (Biological and Chemical Oceanography Data Management Office) site https://www.bco-dmo.org/dataset/852569

temperature. We emphasize the importance of using adapted communities in natural environmental gradients to test climate predictions and hypothesize that mortality defenses are a significant selection criterion in balanced oligotrophic systems.

Most climate change models predict expanding areas of ocean oligotrophy due to increasing thermal stratification and reduced nutrient input to the euphotic zone (Behrenfeld et al. 2006). Such conditions favor photosynthetic bacteria and small eukaryotes (EUK) that dominate phytoplankton communities in warm low-nutrient seas, but how these populations will adapt to and function under warmer conditions remains highly uncertain. On one hand, strong temperature enhancement of growth is predicted by various empirical and theoretical relationships (Eppley 1972; Allen et al. 2005; Sherman et al. 2016). The Q_{10} for picophytoplankton growth (= 2.3; Stawiarski et al. 2016) is at the high end of these estimates. On the other hand, temperature sensitivity of phytoplankton photosynthesis and respiration may be greatly suppressed when nutrients are limited (Marañón et al. 2018). Warming stimulation of protistan grazing or viral infection could also drive the selection for lineages with cell-surface properties or chemical defenses that reduce mortality pressure (Waterbury and Valois 1993; Monger et al. 1999; Strom et al. 2003, 2012), allowing population maintenance at slower growth than predicted by general temperature functions. Ultimately, the most effective strategies for existing or dominating in warmer oligotrophic oceans will be determined in microbial systems with closely coupled rates of production, mortality and nutrient cycling processes. The outcomes may be difficult to determine from experiments with cultures grown for generations on prescribed media without predators, or even from naturally collected communities challenged by environmental conditions not yet experienced. As an alternative, experimental observations along natural environmental gradients that bridge future conditions in the contemporary ocean can provide valuable insights into the net effects of the interdependent factors that affect growth.

The Indian Ocean (IO) receives excess heat from the Pacific through the Indonesian Throughflow (ITF), the only low latitude connection between oceans, and is the fastest warming ocean over the past two decades (Lee et al. 2015; Desbruyères et al. 2017). Over the same period, IO waters also account for most of the global decline in satellite-estimated ocean productivity (Gregg and Rousseux 2019). We investigated microbial food-web interactions along a transect in the eastern IO in 2019 and here report biomass (B), production (P), and growth rate estimates for photosynthetic bacteria and small EUK along an oligotrophic thermal gradient of 10°C. Contrary to the null hypothesis of a consistent and relatively strong thermal enhancement, P : B responses were different, with *Prochlorococcus* (PRO) showing no significant change in biomass turnover over the gradient, *Synechococcus* (SYN) showing a significant but lower-than-expected growth increase, and photosynthetic EUK exhibiting strong variability and negative rates suggestive of elevated viral lysis in high-temperature and high-light waters. These picoplankton groups appear to face different challenges and may have different selected solutions for adapting to warmer ocean conditions.

Materials and methods

Study site and experimental setup

Sampling and experiments were conducted on *R/V Investigator* cruise IN2019V03 (17 May to 05 June 2019) on a south-to-north transect along longitude 110°E, west of Australia (Fig. 1; Landry et al. 2020). The present study considers 17 stations (35–11.5°S) located north of the subtropical front, where the euphotic zones were similarly oligotrophic and well mixed to at least the penetration depth of 7.6% incident light (% I_o measured as PAR, photosynthetically active radiation). Stations were occupied on successive days, with sampling done on a consistent daily schedule, followed by late-night transit between stations. Mean light extinction coefficients determined from morning CTD hydrocasts were used to compute sampling depths corresponding to the transmission characteristics of calibrated shipboard incubators. Experimental water was collected on the evening (~ 21:00 local) hydrocasts at depths corresponding to 75.6%, 31.7%, 18.0%, and 7.6% I_o. Deeper samples (< 3% I_o) are excluded because they were below the layer of uniform mixing and included the upper nitracline at some stations.

For each depth, we prepared a two-treatment dilution experiment (Landry et al. 2008, 2011), with one polycarbonate bottle (2.7 liters) containing unfiltered seawater (100%) and the second (diluted) bottle consisting of ~ 33% whole seawater with filtered water from the same depth. Seawater was filtered directly from the Niskin bottles using a peristaltic pump, silicone tubing and an in-line 0.2-μm Suporcap filter capsule that had previously been acid washed. Dilution bottles were first given a measured volume of filtered water and then gently filled to the top with unscreened water from the Niskin bottles to avoid physical damage to fragile protists. Consistent with previous open-ocean studies with the two-treatment method (Landry et al. 2008, 2011), nutrients were not added to the incubation bottles. In the oligotrophic Sargasso Sea, nutrient additions suppressed grazing and were not necessary for linearity (Lessard and Murrell 1998). Each bottle was subsampled for flow cytometry (FCM) analysis (2 mL) for initial microbial concentrations, and the bottles were placed in their respective light boxes for 24 h, cooled with constant high flow from the ship's running seawater line. The incubators were covered to protect from deck

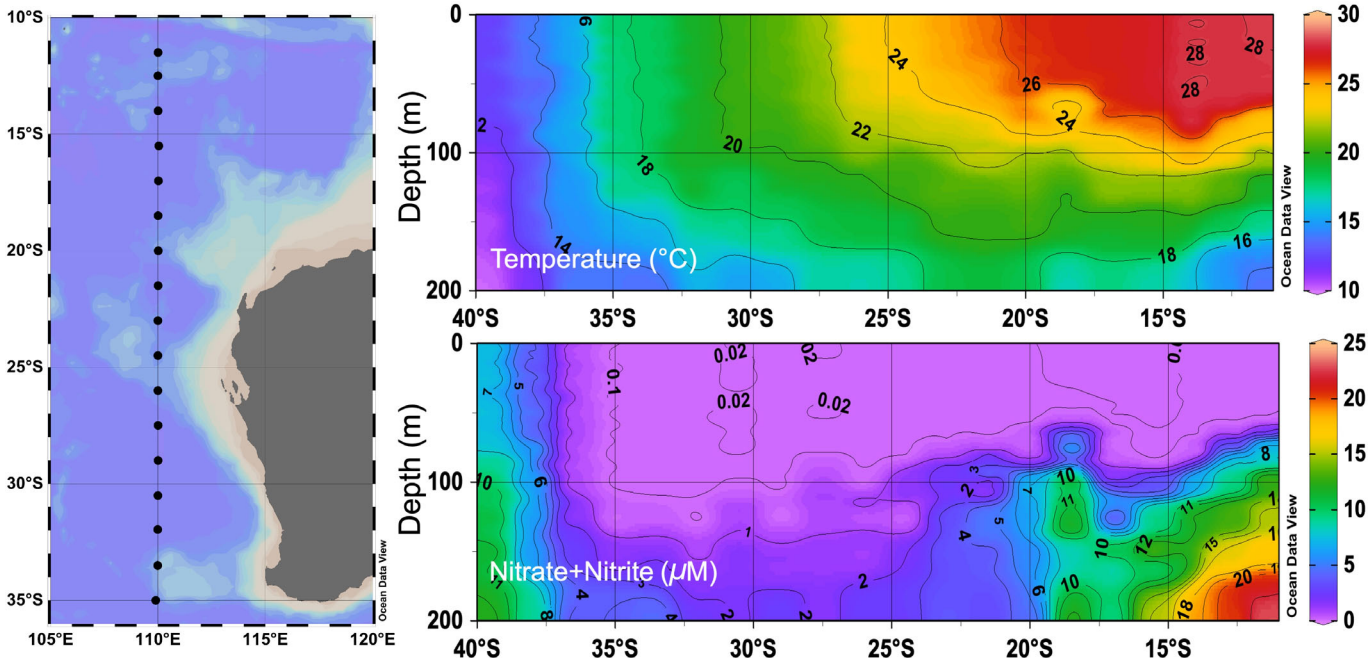

Fig. 1. Study area map with contour plots of temperature (°C) and nutrients (nitrate + nitrite, μM) along 110°E, west of Australia.

lighting during nighttime operations and received full solar lighting during the daytime.

Environmental measurements

We distinguish between measurements that represent experimental incubation conditions vs. the water's prior history at the collection station on the previous day. Temperature and salinity were measured during sample collection by CTD sensors and direct shipboard analyses (Guildline 8400B salinometer). Incubation temperature is the mean of two sensors in the ship's running seawater line, recorded at 5-min intervals and daily averaged. Daily incident solar light (PAR, moles photon flux m^{-2} d^{-1} = Ei m^{-2} d^{-1}) is the mean of two Licor LI-190 PAR sensors positioned on the ship's port and starboard sides, integrated over the photoperiod from measured μEi m^{-2} s^{-1} at 5-min intervals. Wind speed was also measured by two instruments (RM Young 05106 Propellor anemometer, Gill WindObserver II Ultrasonic anemometer), averaged for the daytime as an indicator of day-to-day variability in wind mixing energy. Nutrients were analyzed on board by the CSIRO hydrochemistry group using a Seal AA3HR segmented-flow autoanalyzer (Rees et al. 2018). Analyses were standardized to certified reference material and had detection limits of 0.02 μM for nitrate + nitrite and phosphate, 0.2 μM for silicate, and 0.01 μM for ammonium.

Population biomass and production

Picophytoplankton FCM samples were preserved with 3% paraformaldehyde and frozen at −80°C. Thawed samples were stained with Hoechst 34580 (1 μg mL^{-1}) and analyzed at a flow rate of 30 μL min^{-1} with a Beckman-Coulter CytoFLEX-S instrument with four lasers (Selph 2021). Side scatter, forward angle light scatter (FALS), and fluorescence signals were collected using laser excitation (EX)/emission (EM) filters of EX375/EM450 ± 45 for Hoechst-stained DNA, EX488/EM690 ± 50 for chlorophyll (Chl), and EX561/EM585 ± 42 for phycoerythrin. Listmode files (FCS 3.0) were analyzed with FlowJo software (v.10.6.1) for abundances of PRO, SYN, and EUK and their normalized fluorescence and scatter signals relative to fluorescent bead standards.

Population carbon estimates were determined from cell abundances and mean cell carbon scaled to relative cell sizes. For PRO, we assumed a base value of 32 fg C $cell^{-1}$ and a mean diameter of 0.65 μm for subtropical surface waters. Base values for SYN and EUK were scaled proportionally to 155 and 3150 fg C $cell^{-1}$ for cells of 1.1 and 3.0 μm diameters, respectively. To account for potential cell carbon variability along the transect, we used the bead-normalized FALS ratio $(FALS_i/FALS_b)^{0.55}$ as a measure of the relative cell biovolume in sample i compared to the base value b (Landry et al. 2003), which derives from the near-linear relationship between FALS and Mie scattering cross section for cells in the submicron-micron size range (DuRand and Olson 1996). We also use bead-normalized red fluorescence captured by filter EM690 ± 50 as a relative measure of cell Chl *a* content.

For each dilution experiment, net rates of population growth from initial and final FCM samples in diluted (k_d) and undiluted (k) treatments were used to compute rate estimates of microzooplankton grazing mortality (m, d^{-1}) and instantaneous growth rate (μ, d^{-1}) as: $m = (k_d - k)/(1 - D)$ and $\mu = k + m$, where $D = 0.33$ is the mean measured dilution

factor (Landry et al. 2008; Landry and Selph 2021). Carbon-based estimates of production (P) were calculated from growth and grazing rates and initial estimates of population carbon (B_o) as:

$$P\left(\text{mg C m}^{-3}\,\text{d}^{-1}\right) = \mu \times B_o\left(e^{(\mu-m)t}-1\right)/(\mu-m)t \qquad (1)$$

For each station, population biomass and production estimates are presented as the mean ± standard error, treating the experiments from four light depths as replicates. At 12.5°S, however, only three production estimates are averaged because a deep euphotic zone sample was mistakenly incubated at the highest (76%) light. P : B ratios are computed from depth-integrated values of P and B from the surface to the 7.6% light depth.

Results

An oligotrophic thermal gradient

The 110°E transect bridged two distinct water masses of the eastern IO. The high-salinity (> 35.7 psu) water between 35°S and 27.5°S (Table 1) is subtropical water of the South Indian Central region (Rochford 1977). The warmer low-salinity (< 34.3 psu) water north of 14°S is tropical surface water that enters the IO from the Pacific via the ITF. The intermediate area of T-S properties is a mixing region. During our sampling, the interactions of these waters created a strong thermal gradient of ~ 10°C between southern subtropical (~ 18°C) and tropical (28°C) waters. The 7.6% light depth for experimental sampling varied from 44 to 70 m and averaged 55.5 ± 1.8 m. Physical and chemical variables (T, S, and nutrients) were well mixed to at least this light depth and usually deeper. Mean nitrate + nitrite concentrations were 0.03 μM or less at all stations except 35°S (closest to the subtropical front, where the nutricline breaks the surface), and ammonium (not shown) was below the 0.01 μM detection limit. Excess ratios of phosphate and silicate relative to nitrate + nitrite are indicative of strong nitrogen limitation.

Biomass, production, and growth relationships

While population biomasses were not as uniformly distributed in the mixed layer as physical variables, none of the four sampling depths differed significantly relative to the mixed-layer mean for the transect as a whole. PRO dominated biomass at stations north of 32°S and was consistently 6–10 mg C m^{-3} through the tropical and mixing regions (< 27.5°S; Table 1). SYN and EUK biomasses were lowest in the mixing region and at least twofold higher, on average, at the southern and northern ends. All populations had highest biomass in tropical waters, though at different stations.

Production estimates for PRO and SYN closely follow latitudinal trends for biomass and have relatively small uncertainty estimates despite being experiments from different depths and light levels (Table 2). The latter result is consistent with observations from the equatorial Pacific, where phytoplankton typically has maximal growth at light levels down to ~ 10% I_o before declining with depth (Landry et al. 2011). The similarity of production and biomass trends is verified by the depth-integrated P : B ratios, which are relatively flat with respect to the latitudinal temperature gradient (Fig. 2, upper panels). The P : B slope is not different from zero for PRO ($p > 0.74$), but P : B for SYN shows a relative rate increase ($p < 0.025$) that corresponds to a Q_{10} of 1.36. That P : B increase, however, involves a substantial change in incident PAR over the transect, from < 20 Ei m^{-2} d^{-1} for most of the cooler subtropical stations to ~ 36–37 Ei m^{-2} d^{-1} for most of the warmer northern stations. The P : B-temperature relationship for EUK is insignificant due to substantial variability, including negative production, in the warmest (27–28°C) waters. At stations with negative rates (18.5°S and 14°S), EUK cells declined dramatically between initial and final (post-incubation) FCM cell counts, most notably at highest light (76% I_o). In the flow cytograms, the cells disappeared completely rather than merging with other count categories.

The P : B temperature trends are largely determined by instantaneous growth rates, the major term in the production rate calculations (Eq. 1). Growth rates for PRO average 0.53 d^{-1}, with an insignificant temperature relationship ($p > 0.30$; Fig. 2, bottom). SYN shows a 43% growth rate increase from 0.58 to 0.82 d^{-1} over the 10°C gradient ($p < 0.004$), while EUK growth is highly variable (−0.45 to 0.95 d^{-1}) at 27–28°C with no temperature trend overall.

Bead-normalized scattering and fluorescence properties indicate significant variability in cell carbon and Chl *a* content over the transect (Fig. 3). PRO cell C declines 25% (38.2–30.6 fg C $cell^{-1}$) from the most southern to northern stations while cell Chl *a* declines more dramatically by 3.1 fold. SYN Chl *a* content similarly declines by substantially more (3.7 fold) than the 44% (185–133 fg C $cell^{-1}$) decrease in cell C. EUK shows no clear latitudinal trends in cellular C and Chl *a*, but the ratio of red fluorescence to C is ~ 65% lower on the northern end compared to the most southern station.

Discussion

Temperature effects on growth rates

Ocean ecosystem models generally parameterize phytoplankton temperature sensitivity as a rate doubling for every 10°C increase ($Q_{10} = 2.0$; e.g., Marinov et al. 2010), based primarily on lab studies (Eppley 1972; Stawiarski et al. 2016). More formally, the Metabolic Theory of Ecology predicts an activation energy (E_a) of 0.32 eV for phytoplankton growth (Allen et al. 2005). Our results for adapted communities along a natural oligotrophic temperature gradient are substantially lower. The temperature trends for PRO are insignificant, but regression calculations for 18°C and 28°C give nominal Q_{10} values of 1.06 and 1.18 for P : B and μ, respectively, which

Table 1. Environmental variables and picoplankton biomass in the mixed layer along the 110°E transect in May–June 2019. Temperature, salinity, dissolved nutrients, and biomass are the means of independent measurements at four sampled light depths from 76% to 7.6% I_o. Incident PAR and wind velocity were each measured by two instruments. Uncertainties are standard errors of mean values.

Lat	Temp	Salinity	PAR	Wind	Dissolved nutrients (μM)			Population biomass (mg C m^{-3})		
(°S)	(°C)	(psu)	(Ei m^{-2} d^{-1})	(km h^{-1})	$NO_3 + NO_2$	PO_4	SiO_2	PRO	SYN	EUK
35.0	17.7±0.0	35.84±0.00	20.4±0.1	40.7±0.1	0.05±0.00	0.06±0.00	1.10±0.00	2.31±0.03	0.87±0.03	5.98±0.41
33.5	18.1±0.0	35.91±0.00	15.2±0.1	25.8±0.1	0.03±0.00	0.06±0.00	1.40±0.00	3.06±0.06	0.70±0.05	5.79±0.08
32.0	19.5±0.0	35.99±0.00	18.7±0.1	12.6±0.1	0.03±0.00	0.04±0.00	1.70±0.00	3.10±0.13	0.63±0.02	5.66±0.54
30.5	20.3±0.0	35.91±0.00	16.8±0.4	18.2±0.2	0.02±0.00	0.03±0.00	2.03±0.03	5.87±0.08	0.75±0.01	3.26±0.08
29.0	20.6±0.1	35.87±0.03	19.0±0.5	27.7±0.2	0.03±0.00	0.03±0.00	2.08±0.06	4.89±0.17	0.43±0.02	2.95±0.33
27.5	21.6±0.1	35.75±0.03	17.7±0.4	36.2±0.1	0.03±0.00	0.03±0.00	2.15±0.03	5.35±0.54	0.79±0.16	3.60±0.61
26.0	23.4±0.1	35.50±0.02	28.4±1.9	36.2±0.3	0.02±0.00	0.03±0.00	2.38±0.03	7.25±0.19	0.31±0.01	2.61±0.14
24.5	24.1±0.1	35.41±0.02	25.8±1.1	17.8±0.0	0.03±0.00	0.03±0.00	2.45±0.03	6.58±0.45	0.34±0.04	2.04±0.25
23.0	24.9±0.1	35.29±0.01	27.6±0.9	12.7±0.3	0.03±0.00	0.04±0.00	2.65±0.03	7.64±0.45	0.33±0.06	2.58±0.27
21.5	25.3±0.2	35.22±0.04	34.4±1.8	19.4±0.3	0.02±0.00	0.05±0.01	2.70±0.16	8.27±0.30	0.37±0.02	2.50±0.42
20.0	26.3±0.1	35.08±0.05	34.3±2.4	19.2±0.4	0.02±0.00	0.06±0.00	2.63±0.08	9.37±0.22	0.35±0.03	2.91±0.41
18.5	26.8±0.0	34.74±0.02	37.4±0.8	29.2±0.1	0.02±0.00	0.04±0.00	1.95±0.13	7.52±0.05	0.34±0.03	3.68±0.24
17.0	27.0±0.0	34.60±0.01	37.3±0.8	40.7±0.1	0.00±0.00	0.03±0.00	1.68±0.03	7.60±0.06	0.29±0.02	4.40±0.81
15.5	27.3±0.0	34.61±0.01	35.7±1.6	36.5±0.0	0.01±0.00	0.04±0.00	1.80±0.00	7.80±0.22	0.35±0.01	2.87±0.24
14.0	28.1±0.0	34.29±0.00	35.8±1.0	31.2±0.1	0.03±0.00	0.07±0.00	2.53±0.03	5.96±0.08	2.46±0.09	9.74±0.53
12.5	27.9±0.0	34.13±0.00	36.0±0.9	24.9±0.1	0.03±0.00	0.05±0.00	2.53±0.03	7.73±0.16	3.55±0.17	4.86±0.19
11.5	28.0±0.0	34.18±0.00	37.6±3.4	19.4±0.4	0.02±0.00	0.05±0.00	2.08±0.03	9.88±0.26	1.07±0.02	3.03±0.14

Table 2. Incubation temperature and incident light conditions and population production estimates from shipboard dilution conducted along the 110°E transect in May–June 2019. Production rates are the means of independent measurements at four sampled light depths from 76% to 7.6% I_o. Temperature and incident PAR were each measured by two instruments. Uncertainties are standard errors of mean values.

	Incubation conditions		Population production (mg C m^{-3} d^{-1})		
Lat (°S)	Temp (°C)	PAR (Ei m^{-2} d^{-1})	PRO	SYN	EUK
35.0	18.12±0.05	15.2±0.1	0.87±0.12	0.54±0.11	1.73±0.40
33.5	19.16±0.05	18.7±0.1	2.09±0.22	0.63±0.10	0.61±0.99
32.0	20.26±0.05	16.8±0.4	2.15±0.13	0.46±0.08	1.62±0.75
30.5	20.69±0.05	19.0±0.5	2.73±0.14	0.55±0.03	0.99±0.44
29.0	21.85±0.05	17.7±0.4	2.95±0.13	0.38±0.04	0.83±0.50
27.5	23.31±0.05	28.4±1.9	3.64±0.60	0.85±0.16	1.38±0.91
26.0	24.06±0.05	25.8±1.1	4.40±0.58	0.27±0.04	0.87±0.67
24.5	24.88±0.05	27.6±0.9	5.91±0.91	0.33±0.06	0.17±0.34
23.0	25.58±0.05	34.4±1.8	3.78±0.39	0.27±0.04	0.53±0.27
21.5	26.44±0.05	34.3±2.4	5.24±0.96	0.29±0.05	1.62±0.25
20.0	26.88±0.05	37.4±0.8	3.38±1.19	0.35±0.06	2.41±0.85
18.5	27.10±0.05	37.3±0.8	3.16±0.48	0.27±0.03	−0.78±0.57
17.0	27.31±0.04	35.7±1.6	3.81±0.69	0.25±0.05	1.19±0.65
15.5	28.01±0.01	35.8±1.0	4.58±0.31	0.44±0.07	2.22±0.39
14.0	28.07±0.05	36.0±0.9	4.59±0.93	2.60±0.34	−1.40±1.99
12.5	28.11±0.05	37.6±3.4	5.57±2.29	2.96±1.15	0.77±1.04
11.5	28.06±0.05	21.1±0.5	5.96±0.34	1.16±0.16	0.23±0.54

correspond to apparent E_a estimates of 0.05 and 0.12 eV. The latter are in the range of low values (0.04–0.11 eV) reported by Marañón et al. (2018) for phytoplankton respiration and photosynthesis under nutrient-limited conditions. Q_{10} and E_a values for SYN (1.36 for P : B, 1.42 for μ, 0.23 and 0.27 eV) are significantly higher, but still below prediction. Liu et al. (2021) also found lower E_a for PRO compared to SYN in natural communities of the western subtropical Pacific subjected to temperatures ± 4°C different from the ambient growth environment. In that case, however, both PRO and SYN substantially exceeded the expected higher $E_a = 0.65$ eV for heterotrophs, a possible indication of thermal stress in the short-term perturbation experiments.

The temperature trends for EUK are ambiguous due to high variability and substantial negative rates at 27–28°C (Fig. 2). The cause for the latter is unknown but consistent with viral infection or spontaneous lysis, which others have found more prevalent for picoeukaryotes than photosynthetic bacteria and exacerbated by high light and temperature (Augusti and Sánchez 2002; Baudoux et al. 2007, 2008; Bidle 2016). This could represent a significant challenge for EUKs in a warming ocean that needs to be better studied. In our experiments, the declines were not triggered by abrupt differences in light or temperature between collection and incubation days (Tables 1 and 2), and they occurred in bottles that had not been screened, filtered or manipulated in any way other than gentle filling. However, decline rates may be exaggerated in bottles incubated for a full day at high-light conditions compared to cells that mix freely in the water column. The peak EUK biomass at 14°S (9.7 mg C m^{-3}) was the station where the sharpest cell decline occurred during incubation. These observations, along with high growth rates measured under similar conditions at adjacent stations, suggest a cyclical phenomenon with alternating periods of stock buildup and depletion.

Since biomass (B_o) cancels in the P : B calculations, our cell carbon estimates do not affect the P : B temperature relationships but do help to quantify size and C : Chl *a* variability underlying the trends (Fig. 3). For example, higher PRO and SYN biomasses in warmer tropical waters involve smaller and more abundant cells, and cell Chl *a* declines disproportionately to C. If harvesting photons was the main determinate of growth, growth could easily double if cells at the high-light tropical stations maintained a proportional C : Chl *a* content to those in the subtropics. For PRO, almost identical mean P : B ratios are achieved at subtropical stations 32–33.5°S and tropical stations 11.5–14°S while mean PAR is 1.78 times higher and the Chl *a* : C ratio is 50% lower in tropical waters. Normalizing production to PAR and Chl *a* : C, comparable growth in the tropics is achieved at ~ 89% of the relative light*Chl *a* product ($1.78 \times 0.5 = 0.89$) than at lower subtropical temperature, implying a 12.6% efficiency increase in converting light to C. Similarly, comparing the same station

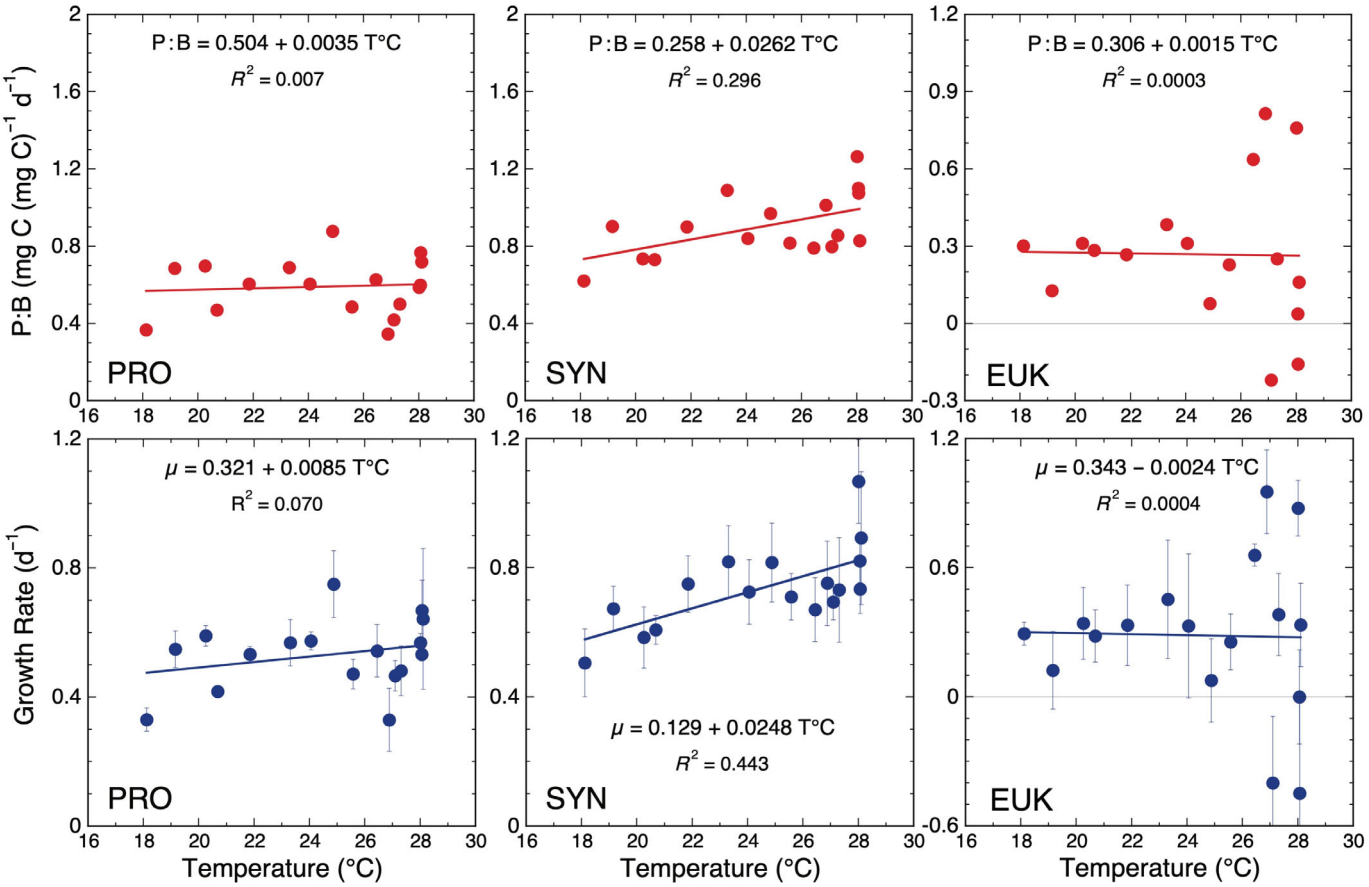

Fig. 2. Production : biomass (P : B) ratios and growth rates for PRO, SYN, and photosynthetic EUK along a 10°C gradient in environmental temperature in the oligotrophic eastern IO. Upper panels (red symbols and lines) are the ratios of depth-integrated carbon biomass and production from the surface to the depth penetration of 7.6% incident PAR. Lower panels (blue symbols and lines) are corresponding mean instantaneous growth rates at four light depths from 76% to 7.6 % *I*o. Uncertainties are standard errors of mean rates.

averages for SYN, 1.22-fold higher P : B is achieved at 1.78 higher PAR and 0.61 relative Chl *a* : C, yielding an almost identical 13.0% efficiency increase that we might attribute to temperature. However, these similar effects manifest differently, with SYN growing faster and PRO downregulating cell Chl *a* more to achieve relatively constant growth.

Because growth rates (μ) are a major part of P : B calculations, they have similar temperature trends (Fig. 2). We highlight the ratio here because the biomass component puts growth into a clearer ecological context and the production calculation (Eq. 1) reminds us that mortality has a role. Regarding context, PRO is the clear biomass and production dominant (Tables 1 and 2) despite faster SYN growth at all stations. Dominance structure is thus not explained only by factors (light, nutrients, temperature) that affect growth rate directly. The maintenance of high PRO biomass in tropical waters (Table 1) despite an expected temperature increase in heterotroph C demand and grazing pressure (Chen et al. 2012) suggests the need for a mechanism that keeps mortality in check.

Hypotheses to explain the experimental results

Several hypotheses can be advanced to explain the present experimental results. On the growth side, for example, flat growth of PRO along the transect could occur if higher nutrient supply rate in the subtropics offsets the higher light and temperature conditions in tropical waters. This hypothesis is inconsistent with the ITF being a major regional source of nutrients and with established N-S trends in plankton biomass and productivity along 110°E (Ayers et al. 2014; Landry et al. 2020 and citations therein). The shallower nitracline in tropical water (Fig. 1) further suggests the potential for higher N supply to the euphotic zone in this area, and there is little reason to expect that PRO would be competitively disadvantaged relative to SYN by trace element limitation. Thus, all components (temperature, light, nutrients) of the "integrated growth environment" (Behrenfeld et al. 2008) appear to favor higher PRO growth in tropical waters.

On the mortality side of the equation, reduced cell size (Fig. 3) could provide some predation relief in warmer water. For bacterial prey and small flagellate consumers, clearance

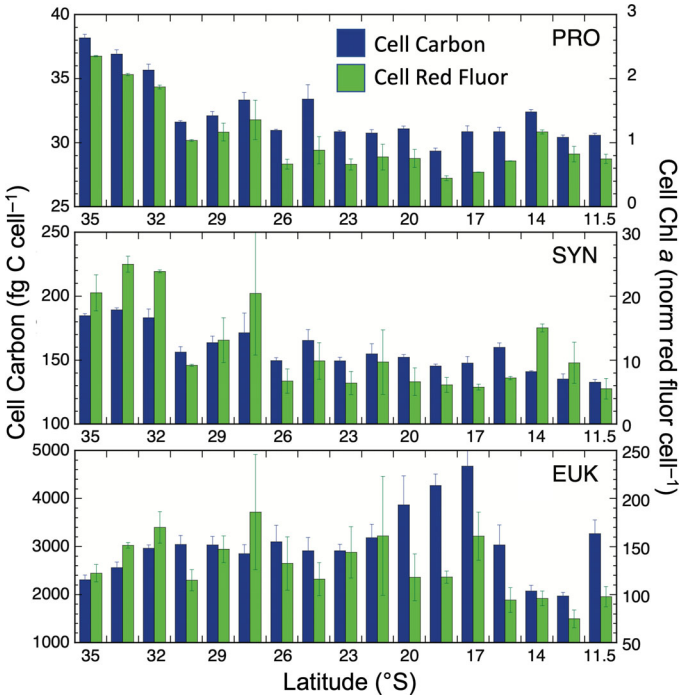

Fig. 3. Variability of cell carbon (fg C cell^{-1}) and Chl *a* indices (normalized red fluorescence cell^{-1}) for PRO, SYN, and photosynthetic EUK along the 110°E transect in the IO. Cell carbon estimates are referenced to FALS for the means of samples collected from upper mixed layer to 7.6% *Io*. Relative values of Chl *a* cell^{-1} are red fluorescence cell^{-1} referenced to bead-normalized red fluorescence. Uncertainties are standard errors of mean values.

rates vary proportionally with prey radius, consistent with the predicted balance of hydrodynamic and surface forces at small scales (Monger and Landry 1991). From transect estimates of cell biovolumes, this equates to 8% reduced predation for PRO, but a slightly higher 11% reduction for SYN. Thus, subject to the same consumers, PRO should benefit generally by being smaller than SYN, with lower overall grazing losses allowing population maintenance at lower growth rates, but the latitudinal trend in cell size does not favor PRO in a relative sense or compensate for the large expected temperature increase in grazing pressure (Chen et al. 2012).

In contrast to the above mechanisms, which offer little to explain how growth and mortality of PRO can remain balanced despite little temperature enhancement of growth, the answer might lie in selection of specific properties that reduce mortality. This recognizes that in nutrient-deficient waters at steady state, where growth is fueled by recycled nutrients driven by biomass turnover, equally viable microbial strategies can emerge from selection of trade-offs in the interdependent processes. The one we consider here, involving cell surface properties, has support in documented predation defense effectiveness for bacterial-sized organisms. For example, Dadon-Pilosof et al. (2017) demonstrated that hydrophilic cell surface of the abundant but slow-growing SAR11, the so-called Teflon bacteria, significantly reduces contact capture by filter-feeding tunicates relative to co-occurring microbes. Previously, Monger et al. (1999) documented substantial variability in cell surface hydrophobicity of PRO cultures and natural assemblages. Hydrophilic variants experienced significantly reduced mortality from protistan grazers, suggesting a twofold range in grazer vulnerability for the measured spectrum of variability. Mixed-layer PRO dominants in that subtropical Pacific study were on the hydrophobic end of the spectrum, more vulnerable to grazers. We hypothesize that a shift in selective advantage from hydrophobic surfaces in subtropical waters to hydrophilic surfaces in tropical waters could account for the relative constancy of PRO growth over the 110°E subtropical-tropical gradient.

Implicit in the above hypotheses is the likelihood that population and trait variability along 110°E taps a deep pool of genetic diversity. The eastern IO is a global biodiversity center at the confluence of many of the ocean's warmest and most impoverished waters and reasonably draws from the federation of cell types (Biller et al. 2015) adapted to each source environment. This highlights our point that the physiological, genetic, and ecological responses of microbial communities to warming ocean conditions will be difficult to predict from laboratory cultures or short-term field perturbation experiments. Existing gradients of adapted complex communities like the eastern IO are natural laboratories for observation and hypothesis testing to improve understanding of the general trends and subtleties of future changes.

References

Agustí, S., and M. C. Sanchez. 2002. Cell viability in natural phyto- plankton communities quantified by a membrane permeability probe. Limnol. Oceanogr. **47**: 818–828. doi:10.4319/lo.2002.47.3.0818

Allen, A. P., J. F. Gillooly, and J. H. Brown. 2005. Linking the global carbon cycle to individual metabolism. Funct. Ecol. **19**: 202–213. doi:10.1111/j.1365-2435.2005.00952.x

Ayers, J. M., P. G. Strutton, V. J. Coles, R. R. Hood, and R. J. Matear. 2014. Indonesian throughflow nutrient fluxes and their potential impact on Indian Ocean productivity. Geophys. Res. Lett. **41**: 5060–5067. doi:10.29037/ajstd.596

Baudoux, A. C., M. J. Veldhuis, H. J. Witte, and C. P. Brussaard. 2007. Viruses as mortality agents of picophytoplankton in the deep chlorophyll maximum layer during IRONAGES III. Limnol. Oceanogr. **52**: 2519–2529. doi:10.4319/lo.2007.52.6.2519

Baudoux, A. C., M. J. W. Veldhuis, A. A. M. Noordeloos, G. van Noort, and C. P. D. Brussaard. 2008. Estimates of virus vs. grazing induced mortality of picophytoplankton in the North Sea during summer. Aquat. Microb. Ecol. **52**: 69–82. doi:10.3354/ame01207

Behrenfeld, M. J., K. H. Halsey, and A. J. Milligan. 2008. Evolved physiological responses of phytoplankton to their

integrated growth environment. Phil. Trans. R. Soc. B **363**: 2687–2703. doi:10.1098/rstb.2008.0019

Behrenfeld, M. J., and others. 2006. Climate-driven trends in contemporary ocean productivity. Nature **444**: 752–755. doi:10.1038/nature05317

Bidle, K. D. 2016. Programmed cell death in unicellular phytoplankton. Current Biol. **26**: R594–R607. doi:10.1016/j.cub.2016.05.056

Biller, S. J., P. M. Berube, D. Lindell, and S. W. Chisholm. 2015. *Prochlorococcus*: The structure and function of collective diversity. Nat. Rev. Microbiol. **13**: 13–27. doi:10.1038/nrmicro3378

Chen, B., M. R. Landry, B. Huang, and H. Liu. 2012. Does warming enhance the effect of microzooplankton grazing on marine phytoplankton in the ocean? Limnol. Oceanogr. **57**: 519–526. doi:10.4319/lo.2012.57.2.0519

Dadon-Pilosof, A., and others. 2017. Surface properties of SAR11 bacteria facilitate grazing avoidance. Nature Microbiol. **2**: 1608–1615. doi:10.1038/s41564-017-0030-5

Desbruyères, D., E. L. McDonagh, B. A. King, and V. Thierry. 2017. Global and full-depth ocean temperature trends during the early 21st century from Argo and repeat hydrography. J. Climate **30**: 1985–1997. doi:10.1175/JCLI-D-16-0396.1

DuRand, M. D., and R. J. Olson. 1996. Contributions of phytoplankton light scattering and cell concentration changes to diel variations in beam attenuation in the equatorial Pacific from flow cytometric measurements of pico-, ultra- and nanoplankton. Deep-Sea Res. II **43**: 891–906. doi:10.1016/0967-0645(96)00020-3

Eppley, R. W. 1972. Temperature and phytoplankton growth in the sea. Fish. Bull. **70**: 1063–1085.

Gregg, W. W., and C. S. Rousseux. 2019. Global ocean primary production trends in the modern ocean color satellite record (1998-2015). Environ. Res. Lett. **14**: 124011. doi:10.1088/1748-9326/ab4667

Landry, M. R., S. L. Brown, J. Neveux, C. Dupouy, J. Blanchot, S. Christensen, and R. R. Bidigare. 2003. Phytoplankton growth and microzooplankton grazing in high-nutrient, low-chlorophyll waters of the equatorial Pacific: Community and taxon-specific rate assessments from pigment and flow cytometric analyses. J. Geophys. Res. **108**: 8142. doi:10.1029/2000JC000744

Landry, M. R., S. L. Brown, Y. M. Rii, K. E. Selph, R. R. Bidigare, E. J. Yang, and M. P. Simmons. 2008. Depth-stratified phytoplankton dynamics in Cyclone *Opal*, a subtropical mesoscale eddy. Deep-Sea Res. II **55**: 1348–1359. doi:10.1016/j.dsr2.2008.02.001

Landry, M. R., R. R. Hood, and C. H. Davies. 2020. Mesozooplankton biomass and temperature-enhanced grazing along a 110°E transect in the eastern Indian Ocean. Mar. Ecol. Prog. Ser. **649**: 1–19. doi:10.3354/meps13444

Landry, M. R., and K. E. Selph. 2021. Pico-phytoplankton abundance, growth and grazing rates along 110°E in the eastern Indian Ocean. doi:10.6076/D17C7J.

Landry, M. R., K. E. Selph, A. G. Taylor, M. Décima, W. M. Balch, and R. R. Bidigare. 2011. Phytoplankton growth, grazing and production balances in the HNLC equatorial Pacific. Deep-Sea Res. II **58**: 524–535. doi:10.1016/j.dsr2.2010.08.011

Lee, S.-K., W. Park, M. O. Baringer, A. Gordon, B. Huber, and Y. Liu. 2015. Pacific origin of the abrupt increase in Indian Ocean heat content during the warming hiatus. Nature Geosci. **8**: 445–450. doi:10.1038/NGEO2438

Lessard, E. J., and M. C. Murrell. 1998. Microzooplankton herbivory and phytoplankton growth in the northwestern Sargasso Sea. Aquat. Microb. Ecol. **16**: 173–188. doi:10.3354/ame016173

Liu, K., K. Suzuki, B. Chen, and H. Liu. 2021. Are temperature sensitivities of *Prochlorococcus* and *Synechococcus* impacted by nutrient availability in the subtropical northwest Pacific? Limnol. Oceanogr. **66**: 639–651. doi:10.1002/lno.11629

Marañón, E., M. P. Lorenzo, P. Cermeño, and B. Mouriño-Carballido. 2018. Nutrient limitation suppresses the temperature dependence of phytoplankton metabolic rates. ISME J. **12**: 1836–1845. doi:10.1038/s41396-018-0105-1

Marinov, I., S. C. Doney, and I. D. Lima. 2010. Response of ocean phytoplankton community structure to climate change over the 21st century: partitioning the effects of nutrients, temperature and light. Biogeosci. **7**: 3941–3959. doi:10.5194/bg-7-3941-2010

Monger, B. C., and M. R. Landry. 1991. Prey-size dependency of grazing by free-living marine flagellates. Mar. Ecol. Prog. Ser. **74**: 239–248. doi:10.3354/meps074239

Monger, B. C., M. R. Landry, and S. L. Brown. 1999. Feeding selection of heterotrophic marine nanoflagellates based on the surface hydrophobicity of their picoplankton prey. Limnol. Oceanogr. **44**: 1917–1927. doi:10.4319/lo.1999.44.8.1917

Rees, C., L. Pender, K. Sherrin, C. Schwanger, P. Hughes, S. Tibben, A. Marouchos, and M. Rayner. 2018. Methods for reproducible shipboard SFA nutrient measurement using RMNS and automated data processing. Limnol. Oceanogr.: Methods **17**: 5–41. doi:10.1002/Iom3.10294

Rochford, D. J. 1977. Further studies of plankton ecosystems in the eastern Indian Ocean. II. Seasonal variations in water mass distribution (upper 150 m) along 110°E. (August 1962-August 1963). Aust. J. Mar. Freshw. Res. **28**: 541–555. doi:10.1071/MF9770541

Selph, K. E. 2021. Enumeration of marine microbial organisms by flow cytometry using near-UV excitation of Hoechst 34580-stained DNA. Limnol. Oceanogr.: Methods **19**: 692–701.

Sherman, E., J. K. Moore, F. Primeau, and D. Tanouye. 2016. Temperature influence on phytoplankton community

growth rates. Global Biogeochem. Cycles **30**: 550–559. doi:10.1002/2015GB005272

Stawiarski, B., E. T. Buitenhuis, and C. Le Quéré. 2016. The physiological response of picophytoplankton to temperature and its model representation. Front. Mar. Sci. **3**: 164. doi:10.3389/fmars.2016.00164

Strom, S., G. Wolfe, A. Slajer, S. Lambert, and J. Clough. 2003. Chemical defense in the microplankton. II. Inhibition of protist feeding by β-dimethylsulfoniopropionate (DMSP). Limnol. Oceanogr. **48**: 230–237. doi:10.4319/lo.2003.48.1.0230

Strom, S. L., B. Brahamsha, K. A. Fredrickson, J. K. Apple, and A. G. Rodriguez. 2012. A giant cell surface protein in *Synechococcus* WH8102 inhibits feeding by a dinoflagellate predator. Environ. Microbiol. **14**: 807–816. doi:10.1111/j.1462-2920.2011.02640.x

Waterbury, J. B., and F. W. Valois. 1993. Resistance to co-occurring phages enables marine *Synechococcus* communities to coexist with cyanophages abundant in seawater. Appl. Environ. Microbiol. **59**: 3393–3399. doi:10.1128/AEM.59.10.3393-3399.1993

Acknowledgments

We appreciate the contributions of the captain and crew of *R/V Investigator* in facilitating this research and especially thank the CSIRO hydrography/hydrochemistry team for their exceptional efforts in providing CTD and nutrient data. Greg Mitchell and Elliot Weiss provided optical expertise for the construction and calibration of the incubator boxes. Research support was provided by National Science Foundation Grant OCE-1851558, a Murdoch University Distinguished Collaborator Award, and the Hong Kong Branch of Southern Marine Science and Engineering Guangdong Laboratory (Guangzhou; SMSEGL20SC02). Water and plankton samples at 29–23°S, 110°E were taken under Australian Fisheries Management Authority scientific permit 1004152, Australian Government permit AU-COM2019-446 and those in the Abrolhos Marine Park under permit PA2018-00065-1 issued by the Director of National Parks, Australia. The views expressed in this publication do not necessarily represent those of the Director of National Parks, CSIRO, or the Australian Government.

Submitted 11 May 2021
Revised 05 August 2021
Accepted 24 October 2021